reactions

MDPI

Article

Electrolysis of Liquefied Biomass for Sustainable Hydrogen and Organic Compound Production: A Biorefinery Approach

Ana P. R. A. Ferreira [1], M. Margarida Mateus [2,3] and Diogo M. F. Santos [1,*]

[1] Center of Physics and Engineering of Advanced Materials, Laboratory for Physics of Materials and Emerging Technologies, Chemical Engineering Department, Instituto Superior Técnico, Universidade de Lisboa, 1049-001 Lisbon, Portugal; ana.a.ferreira@tecnico.ulisboa.pt
[2] C5Lab-Sustainable Construction Materials Association, Edifício Central Park, Rua Central Park 6, 2795-242 Lisbon, Portugal; mmateus@c5lab.pt
[3] Center for Natural Resources and the Environment (CERENA), Instituto Superior Técnico, Universidade de Lisboa, 1049-001 Lisbon, Portugal
* Correspondence: diogosantos@tecnico.ulisboa.pt

Abstract: Liquefaction is an effective thermochemical process for converting lignocellulosic biomass into bio-oil, a hydrocarbon-rich resource. This study explores liquefied biomass electrolysis as a novel method to promote the electrocracking of organic molecules into value-added compounds while simultaneously producing hydrogen (H_2). Key innovations include utilizing water from the liquefaction process as an electrolyte component to minimize industrial waste and incorporating carbon dioxide (CO_2) into the process to enhance decarbonization efforts and generate valuable byproducts. The electrolysis process was optimized by adding 2 M KOH, and voltammetric methods were employed to analyze the resulting emulsion. The experimental conditions, such as the temperature, anode material, current type, applied cell voltage, and CO_2 bubbling, were systematically evaluated. Direct current electrolysis at 70 °C using nickel electrodes produced 55 mL of H_2 gas with the highest Faradaic (43%) and energetic (39%) efficiency. On the other hand, pulsed electrolysis at room temperature generated a higher H_2 gas volume (102 mL) but was less efficient, showing 30% Faradaic and 11% energetic efficiency. FTIR analysis revealed no significant functional group changes in the electrolyte post-electrolysis. Additionally, the solid deposits formed at the anode had an ash content of 36%. This work demonstrates that electrocracking bio-oil is a clean, sustainable approach to H_2 production and the synthesis of valuable organic compounds, offering significant potential for biorefinery applications.

Keywords: liquefied biomass; bio-oil; electrolysis; hydrogen; electrocracking; CO_2 reduction

check for updates

Academic Editor: Dmitry Yu. Murzin

Received: 3 December 2024
Revised: 16 January 2025
Accepted: 31 January 2025
Published: 2 February 2025

Citation: Ferreira, A.P.R.A.; Mateus, M.M.; Santos, D.M.F. Electrolysis of Liquefied Biomass for Sustainable Hydrogen and Organic Compound Production: A Biorefinery Approach. *Reactions* **2025**, *6*, 10. https://doi.org/10.3390/reactions6010010

Copyright: © 2025 by the authors. Licensee MDPI, Basel, Switzerland. This article is an open access article distributed under the terms and conditions of the Creative Commons Attribution (CC BY) license (https://creativecommons.org/licenses/by/4.0/).

1. Introduction

The term "biomass" primarily refers to organic matter derived from plants. Biomass is produced by green plants that transform sunlight into plant material through photosynthesis [1]. Lignocellulosic biomass is the most abundant plant material and, therefore, widely available in high quantities and at a low cost [2]. However, when biomass is used as a raw material, it is crucial to implement reforestation programs because it is not an inexhaustible energy source [1]. Biomass meets various energy needs, such as electricity generation, domestic heating, vehicle fuel, and industrial heating. Despite these applications, biomass is primarily used for direct combustion [3].

The biomass liquefaction process has been introduced as an effective thermochemical method to convert lignocellulosic biomass into liquid products using a solvent [4]. A

key goal of liquefaction is to reduce the oxygen content in biomass, which constitutes 40–50 wt.% of its composition [5]. The resulting bio-oil has a complex composition containing various oxygenated compounds, including acetic acid, ethanol, carboxylic acids, phenols, aldehydes, ketones, alcohols, and esters [3]. Therefore, bio-oil can serve as a biofuel and can also be used to produce bio-polyols, antioxidants, and other chemicals derived from hydrocarbons and lignin [6].

Hydrogen (H_2) is considered a clean fuel for the future, as its combustion generates only water. Moreover, it has an energy density approximately 2.75 times higher than hydrocarbon fuels like gasoline, offering low pollution and versatile applications [3,7]. Water electrolysis is one of the most promising technologies for producing H_2 [7]. This process induces the dissociation of water into H_2 and oxygen (O_2) by applying an electric current [8]. Water electrolysis has been extensively studied due to its potential to enable scalable H_2 production, particularly when coupled with renewable energy sources. In this case, the resulting H_2 is classified as green H_2 [9]. Additionally, among existing carbon dioxide (CO_2) capture technologies, the electrochemical reduction of CO_2 has recently garnered the most interest [10]. This process can capture CO_2 while producing value-added products such as carbon monoxide (CO), formic acid (HCOOH), formaldehyde (HCHO), and methane (CH_4) [11]. When water electrolysis is combined with CO_2 reduction, the resulting co-electrolysis process typically produces syngas, a versatile fuel comprising CO and H_2 that is widely used for energy generation and chemical synthesis [12].

Despite the apparent simplicity of the water electrolysis process, several challenges are delaying the large-scale production of green H_2. These include the large overpotentials required for operating the electrolyzer, thereby increasing electricity costs, or concerns regarding the use of freshwater, which directly competes with agricultural and human consumption. To overcome these limitations, researchers are focusing on new approaches, such as seawater and biomass electrolysis. The former is an exciting alternative, as it leverages abundant seawater and the large-scale deployment of offshore renewable energy; however, current commercial electrolyzers require the prior desalination of seawater, increasing the process costs and creating environmental issues concerning the disposal of concentrated brine [13].

To avoid desalination, researchers are exploring direct seawater electrolysis as a cost-effective method for green H_2 production. A significant challenge remains in developing durable, earth-abundant electrocatalysts that withstand corrosive conditions. Yu et al. have addressed this by fabricating self-supported nickel–iron phosphosulfide (NiFeSP) nanotube array electrocatalysts with excellent activity and durability for hydrogen and oxygen evolution reactions (HER and OER) in simulated alkaline seawater. Additionally, the NiFeSP electrode exhibited promising activity during urea oxidation as an alternative anodic process during hybrid seawater electrolysis [14].

The oxidation of organic matter at the anode allows the replacement of the kinetically hindered OER and the "corrosive" chlorine evolution reaction as the anodic process, with the additional advantage of reducing the voltage required for electrolysis [14,15]. For this reason, researchers are investigating hybrid seawater electrolysis as an innovative and promising approach for green H_2 production, as its more thermodynamically favorable anodic oxidation reaction reduces the electrolysis energy demand while enabling the co-production of valuable chemicals or the elimination of environmental pollutants [15].

Accordingly, a key motivation for studying biomass electrolysis is that the oxidation of oxygenated organic species from biomass can reduce the electrolysis cell voltage below 1.23 V. Various organic molecules can be utilized in the anodic process, enabling the direct valorization of agricultural and forestry waste (lignocellulosic materials) and by-products from biofuel industries [16]. Recently, Umer et al. carried out $FeCl_3$-mediated

biomass electrolysis using different biomass feedstocks (i.e., glucose, starch, lignin, and cellulose) to produce H_2 at ambient temperature using a cell voltage as low as 1.20 V. It was demonstrated that the process could produce H_2 with a higher yield rate and lower electricity consumption than conventional water electrolysis [17].

The term "electrocracking" has also been introduced as a novel concept linking H_2 production with the electrolysis of liquefied biomass. This process involves decomposing organic compounds in the liquefied biomass into lighter hydrocarbons by passing an electric current between two electrodes [18]. Building on this concept, the present study integrates electrocracking with a patented biomass liquefaction technology to explore sustainable pathways for H_2 and organic compound production. Specifically, it investigates the electrolysis of biomass liquefied through an industrial liquefaction process, incorporating water recovered from that process and subsequent CO_2 capture.

The liquefied biomass was supplied by the Portuguese cement group CMP–Cimentos Maceira e Pataias (Secil), which holds a patent for its biomass liquefaction process, named ENERGREEN [19]. The central objective of this pilot-scale facility is to produce a clean and sustainable biofuel with a high calorific value for use in cement kilns, effectively replacing fossil fuels. The feedstock used was *Eucalyptus globulus* sawdust. Through acid liquefaction at 160 °C and atmospheric pressure, and by using 2-ethyl-hexanol as the solvent and *p*-toluenesulfonic acid as the catalyst, the process yields liquefied biomass, polyols, condensates, extraction water, and sugars during the reaction. The final step involves separating the liquefied material into aqueous and organic phases. The aqueous phase is collected in two stages: first, through the condensation of vapors produced during the liquefaction reaction, yielding condensed water, and second, by the liquid–liquid extraction of the biofuel, which also generates an aqueous fraction.

After extracting the sugars, the liquefied biomass was subjected to electrolysis trials, wherein operating parameters such as the temperature, anode material, current type, cell voltage, and the effect of CO_2 sparging were evaluated. Furthermore, fundamental electrochemical analyses, including cyclic voltammetry (CV) and linear scan voltammetry (LSV), were conducted to characterize the redox behavior and stability of the samples under electrolytic conditions. By examining these parameters and performing detailed electrochemical analyses, the present work aims to advance the understanding of biomass electrolysis as a viable pathway for sustainable H_2 and organic compound production, contributing to the development of integrated biorefinery systems.

2. Materials and Methods

2.1. Electrolyte Preparation and Characterization

The liquefied biomass used in this study was supplied directly by CMP–Cimentos Maceira e Pataias (Secil, Portugal) cement group, which produced it from *Eucalyptus globulus* sawdust using their patented process [19]. Previous studies have demonstrated that the ionic conductivity of liquefied biomass solutions can be significantly enhanced by preparing an alkaline emulsion suitable for electrochemical analysis [20]. Based on these findings, this study utilized an emulsion of *Eucalyptus globulus* sawdust liquefied biomass with 2 M KOH aqueous solution (50 vol.%). Tests were also performed using waters from the two distinct phases of the liquefaction process (condensed water and two-phase water). The phases of the two-phase water system were named the light-colored phase and the dark phase.

For both electrolytes, the values of conductivity (σ) and pH were registered. Additionally, the density (ρ) of the emulsion (liquefied biomass + 2 M KOH) was measured, and a humidity content test was conducted using a VWR (IT 1400108) balance. A HANNA Instru-

ments (pH20) device was used for conductivity and pH measurements, and a pycnometer was used for the density measurement.

2.2. Electrochemical Measurements

Cyclic voltammetry (CV) and linear scan voltammetry (LSV) measurements were performed using an ALS 2325 bipotentiostat in a 60 mL electrolytic cell with a thermostatic water jacket for temperature control. A typical three-electrode arrangement was used, comprising a platinum (Pt) disk (A = 0.1256 cm^2) as the working electrode, a Pt mesh (A = 50 cm^2) as the counter electrode, and a saturated calomel electrode (SCE) as the reference electrode. Unless otherwise noted, all potentials are given alongside the SCE reference. For the hydrogen evolution reaction (HER) studies conducted via LSV, two working electrodes were utilized: a Pt electrode with an area of 1 cm^2 and a nickel (Ni) electrode (A = 22.4 cm^2). In CV experiments, the potential was scanned between the open-circuit potential (OCP) and 0.6 V at scan rates ranging from 5 to 1000 mV s^{-1}. Measurements were conducted at room temperature (RT = 17 °C) and 65 °C. For LSV studies focusing on the HER, the potential was scanned at 1 mV s^{-1} from the OCP to −2 V, with tests performed at 25 °C and 70 °C.

2.3. Electrolysis Tests

The electrolysis tests were performed in a small-scale laboratory electrolyzer (300 mL) using PAR 273A computer-controlled potentiostat/galvanostat (Princeton Applied Research, Inc., Oak Ridge, TN, USA) and the associated PowerSUITE package to control the experiments. Gas quantification was performed using a Ritter MilliGascounter (MGC-1 V3.4 PMMQA, Ritter, Bochum, Germany) apparatus. Most electrolysis tests used identical Ni plates (A = 22.4 cm^2) as the cathode and anode. Additional tests were carried out with a Ni plate as the cathode and a TiO_2-RuO_2 alloy anode.

Besides the regular direct current (DC) electrolysis tests, other tests included using an AMI-7001S anion-exchange membrane (Membranes International Inc., Ringwood, NJ, USA), bubbling CO_2 into the electrolyte during electrolysis, and applying alternating current (AC) waves. All these tests used Ni electrodes. Specifically, electrolysis using AC explored two types of wave shapes: half-sinusoidal AC waves and pulsating waves. The wave shape and electrolysis parameters were verified on a TDS 1012B oscilloscope (Tektronix, Beaverton, OR, USA). For the first type of wave, an alternating power supply (230/12 V, 1 A) was used with a diode (ultra-fast rectifier BYV32) to rectify the sinusoidal wave. A microcontroller based on an Atmega328 processor was used for pulse generation, and a code in C language was programmed to control the pulse frequency and duty cycle. The cell voltage applied in these studies was 1.5 V, 2.4 V, and 3 V; temperatures of 25, 50, 60, and 70 °C were tested.

3. Results and Discussion

3.1. Electrolyte Characterization

Table 1 lists the conductivity, pH, density, and humidity data measured for the used solutions.

Table 1. Values of conductivity, pH, density, and humidity for the emulsion prepared and the waters from the liquefaction process.

	σ, mS cm^{-1}	**pH**	**ρ, g dm^{-3}**	**Humidity, %**
Emulsion	115	13.8	1123	78
Condensed water	8.73×10^{-3}	2.51	–	–
Light-colored phase	0.01×10^{-3}	1.53	–	–
Dark phase	11.2	2.09	–	–

3.2. Electrochemical Studies

3.2.1. Cyclic Voltammetry

Figures 1–4 present the CVs on the 50/50 emulsion of liquefied biomass + 2 M KOH run with a Pt electrode at 17 and 65 °C, respectively. Figure 1 shows two oxidation peaks, a_1 at −0.2 V and a_2 at 0.28 V, and one reduction peak, c_1 at −0.45 V. It is also notable that peak a_2 becomes ill-defined as the scan rate increases.

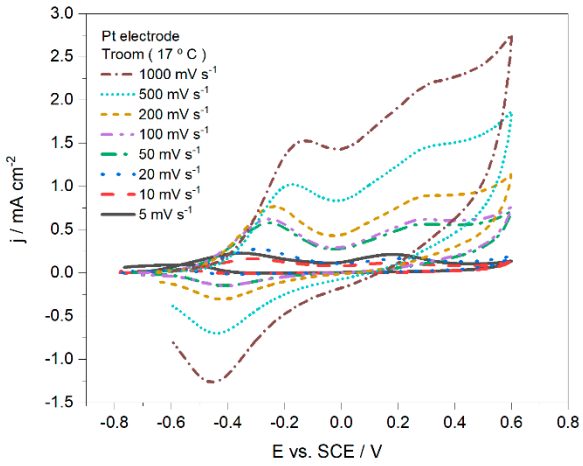

Figure 1. Cyclic voltammograms (CVs) of the 50/50 emulsion of liquefied biomass + 2 M KOH using a Pt working electrode and applying scan rates ranging from 5 to 1000 mV s^{-1} at room temperature (17 °C).

Several hypotheses could explain the presence of these three peaks: (i) the oxidation of two different species, one of which is later reduced; (ii) a two-step oxidation of the same species, which is subsequently reduced; or (iii) the oxidation of one species that undergoes a chemical reaction, generating a different species that is oxidized (corresponding to peak a_2) and then reduced. Regardless of these possibilities, a more detailed investigation of peak c_1 is necessary, as it may be independent of the oxidation peaks, as further elaborated below. To analyze the effect of the scan rate on the system, Figure 2 presents three CVs recorded at different scan rates (5, 50, and 200 mV s^{-1}).

Figure 2A shows that, at a low scan rate (5 mV s^{-1}), in addition to the two oxidation peaks (a_1 and a_2), there is a third oxidation peak (c_2 at −0.6 V) in the backscan. This third anodic peak could result from a diffusional phenomenon. Specifically, after the second anodic peak (a_2), the low scan rate allows sufficient time for the oxidized species on the electrode's surface to diffuse into the bulk solution. Consequently, new species susceptible to oxidation can reach the electrode's surface. The disappearance of peak c_2 and the appearance of peak c_1 at higher scan rates (Figure 2B,C) can be explained conversely: when increasing the scan rate, after the second oxidation peak (a_2), the oxidized species lacks sufficient time to diffuse into the bulk solution, undergoing reduction as more negative potentials are reached.

Going back to Figure 1, the presence of peak c_1 can indicate a possible reversible reaction. In other words, peak c_1 can correspond to the inverse process (i.e., a reduction) of one of the anodic peaks, a_1 or a_2. According to Pacheco et al., when a process is electrochemically reversible, the anodic peak potential does not change with the scan rate [21]. Thus, it would be intuitive to say that the oxidation process in peak a_2 is reversible since its potential is always the same, unlike peak a_1. However, Elgrishi et al. explain that reversibility depends on the scan rate, i.e., for sufficiently high scan rates, all processes can appear as irreversible [22]. Therefore, at low scan rates (Figure 2A), the reduction peak

(c_1) is not present; thus, it cannot be concluded that the oxidation process from peak a_2 is reversible and corresponds to peak c_1.

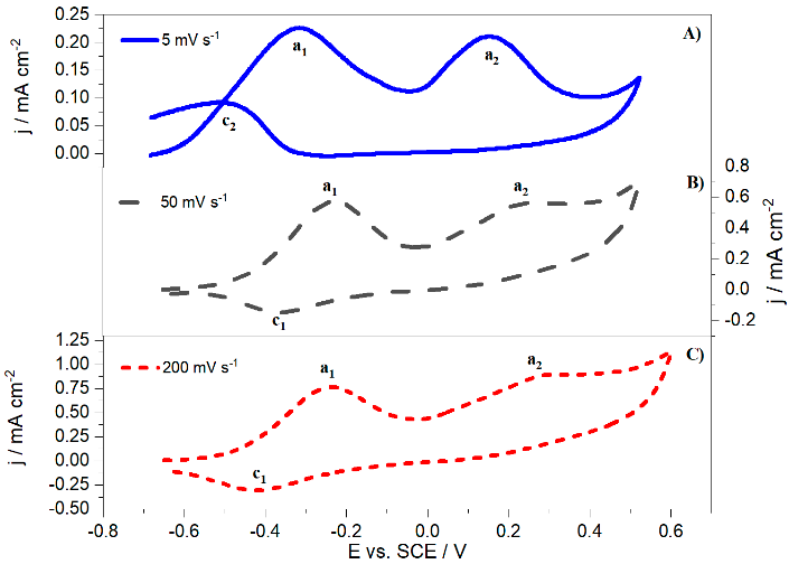

Figure 2. CVs of a 50/50 emulsion of liquefied biomass + 2 M KOH using a Pt working electrode at room temperature (17 °C) and applying scan rates of (**A**) 5 mV s^{-1}, (**B**) 50 mV s^{-1}, and (**C**) 200 mV s^{-1}.

To disprove the hypothesis that peak a_1 is reversible, CVs at different scan rates were run until an upper potential limit of 0.1 V was reached, not reaching the potential necessary for the process represented by peak a_2 to occur (Figure 3).

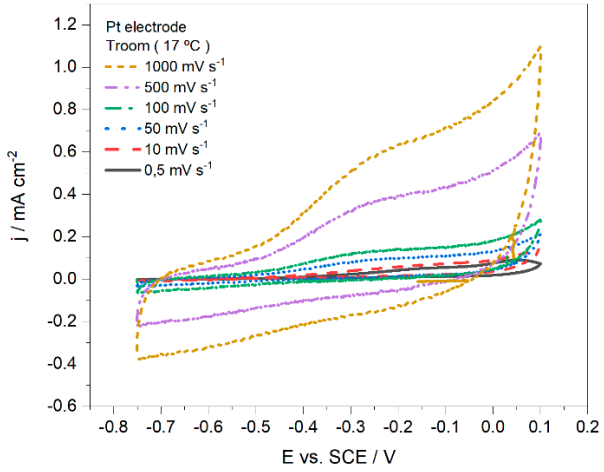

Figure 3. CVs of a 50/50 emulsion of liquefied biomass + 2 M KOH using a Pt working electrode and applying scan rates from 0.5 to 1000 mV s^{-1} at room temperature (17 °C).

Figure 3 clearly shows peak a_1 at −0.2 V; however, peak c_1 is not present. This fact reinforces the assumption that peak c_1 is independent of the oxidation of the species represented in peak a_1. As there is no clear indication of the reversibility of any of the peaks and their dependency on the scan rate, it was decided that the electrochemical equation for irreversible processes would be applied to calculate the relevant kinetic parameters. These uncertainties are expected because irreversibility is more prevalent than reversibility in some redox pairs, including organics [23]. Furthermore, Espinoza et al. claim that oxidative or reductive degradation, dimerization, reaction with solvent, fast mass transport, and other processes that diminish the quantity of the species produced on the electrode's

surface have a strong influence on the CVs, causing asymmetries and even the complete elimination of the anodic and cathodic peaks [23].

The oxidation and reduction peak's current dependency on the scan rate for irreversible processes is given by Equations (1) and (2), respectively,

$$i_p = 0.496\sqrt{(1-\alpha)n_a} \times nFAC\sqrt{(FD\nu)/(RT)} \quad (1)$$

$$i_p = 0.496\sqrt{\alpha n_a} \times nFAC\sqrt{(FD\nu)/(RT)} \quad (2)$$

where i_p is the peak current, n is the number of exchanged electrons, F is Faraday's constant (96,485 C mol^{-1}), A is the Pt disk working electrode's area (0.1256 cm^2), C is the concentration of electrochemically active species in the solution (3.34×10^{-5} mol cm^{-3}), D is the diffusion coefficient of that species (6.98×10^{-9} cm^2 s^{-1}), α is the charge transfer coefficient, n_a is the number of electrons involved in the rate-determining step (being 1 the most likely value), ν is the scan rate in V s^{-1}, R is the universal gas constant (8.314 J K^{-1} mol^{-1}), and T is the temperature in K. Equations (1) and (2) were used to calculate the number of exchanged electrons, n, in the processes represented by peaks a_1, a_2, and c_1, following the determination of the charge transfer coefficient, α. The α coefficient is usually interpreted as being a measure of the position of the transition state of the reaction; in this case, the reduction reaction, and the oxidation reaction, this coefficient is defined as $1 - \alpha$. When the α value is near 1, this implies the transition state is "product-like", and similarly, a value close to zero indicates a "reactant-like" transition state [24]. Thus, Equations (3) and (4) were used to calculate the anodic and cathodic charge transfer coefficients, respectively, for an irreversible redox process [25,26]. The results obtained for n and α at room temperature are shown in Table 2.

$$E_p = (RT)/(2(1-\alpha)n_aF) \times \ln(\nu) + b \quad (3)$$

$$E_p = -(RT)/(2\alpha n_aF) \times \ln(\nu) + b \quad (4)$$

Table 2. Kinetic parameters of the redox processes in the bio-oil emulsion using a Pt electrode at room temperature and 65 °C.

Temperature (°C)	Kinetic Parameters	Peak a_1	Peak a_2	Peak c_1
RT (17 °C)	α	0.61	0.63	0.96
	n	3.1	4.7	2.0
65 °C	α	0.57	–	0.93
	n	4.6	–	1.0

To study the effect of temperature, CVs were also run at 65 °C (Figure 4). Only one anodic peak (a_1), at −0.1 V, can be seen in Figure 4, with a cathodic peak (c_1) at ca. −0.4 V. The presence of a single anodic peak is probably due to the coalescence of peaks a_1 and a_2, shown in Figure 1. The peaks' coalescence should be due to the similarity of oxidation peak potentials at higher temperatures. Since the anodic peak in Figure 4 has a similar potential to peak a_1 in Figure 1, it is plausible that this peak is not influenced by temperature. Considering this hypothesis, it is possible to claim that peak a_2 from Figure 1 shifts to more negative potentials, towards peak a_1. This shift in peak a_2 indicates that the oxidation of the species corresponding to peak a_2 becomes easier at higher temperatures.

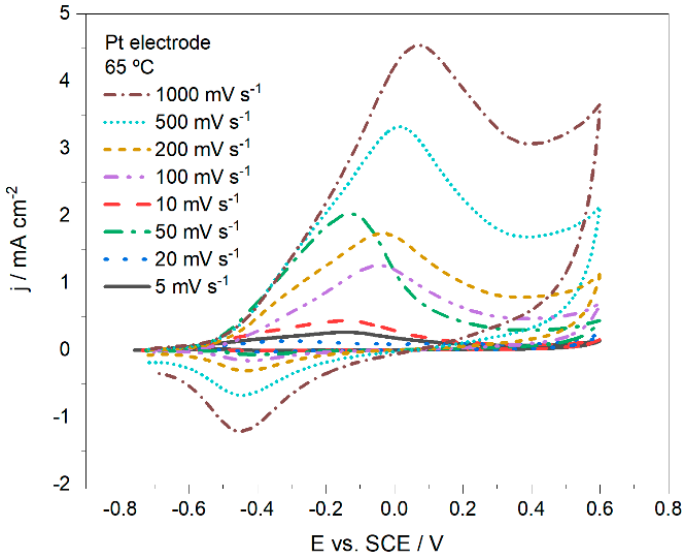

Figure 4. CVs of a 50/50 emulsion of liquefied biomass + 2 M KOH using a Pt working electrode and scan rates of 5 to 1000 mV s^{-1} at 65 °C.

Equations (1)–(4) were also used to calculate the kinetic parameters (n and α) from the data in Figure 4 for the processes denoted as a_1 and c_1 in Figure 5 (Table 2). To better illustrate the influence of the scan rate on the system at 65 °C, CVs at 5, 50, and 200 mV s^{-1} are shown in Figure 5.

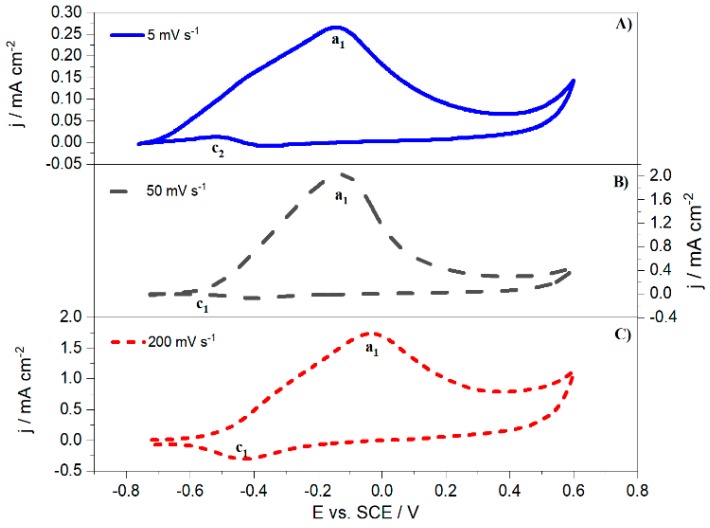

Figure 5. CVs of a 50/50 emulsion of liquefied biomass + 2 M KOH using a Pt working electrode at 65 °C and applying scan rates of (**A**) 5 mV s^{-1}, (**B**) 50 mV s^{-1}, and (**C**) 200 mV s^{-1}.

The system at 65 °C (Figure 5) exhibits a similar trend to the one observed at 17 °C (Figure 2), with the main difference being the disappearance of peak a_2 and the broadening of peak a_1. This can be clearly seen in Figure 6, which shows CVs at two different scan rates to further compare the differences between the results obtained at room temperature (17 °C) and 65 °C. Furthermore, Figure 6 shows that the temperature increase also significantly increases the current density, demonstrating that it is beneficial to carry out liquified biomass electrolysis at temperatures higher than room temperature.

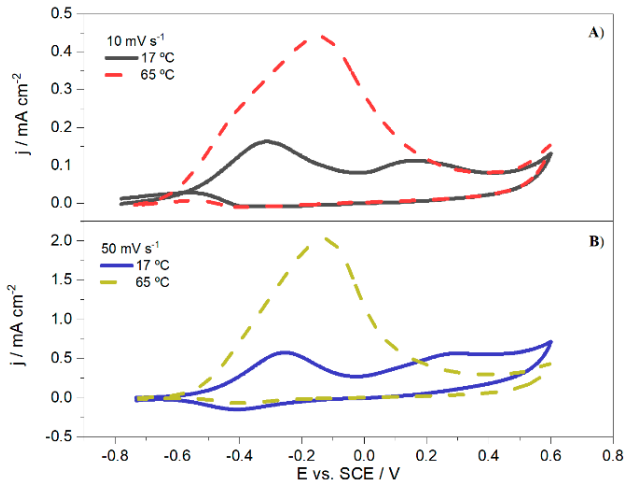

Figure 6. CVs of a 50/50 emulsion of liquefied biomass + 2 M KOH using a Pt working electrode. Effect of temperature (17 and 65 °C) on the CVs at scan rates of (**A**) 10 mV s^{-1} and (**B**) 50 mV s^{-1}.

Lastly, Figure 7 shows CVs when using two different scan rates (10 and 50 mV s^{-1}) for the 50/50 emulsion of liquefied biomass + 2 M KOH before and after a 3 h electrolysis test. It shows that an increase in the current density is recorded with the emulsion after electrolysis and a slight shift in the oxidation peaks towards more positive potentials.

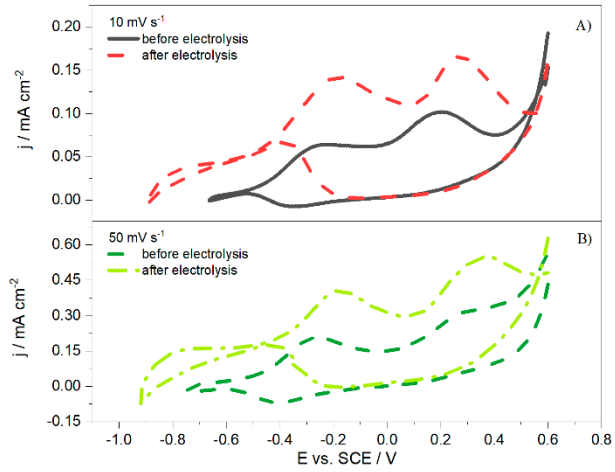

Figure 7. CVs using a Pt working electrode of a 50/50 emulsion of liquefied biomass + 2 M KOH before and after electrolysis at (**A**) 10 mV s^{-1} and (**B**) 50 mV s^{-1}.

The observed current density increase agrees with previous studies using liquefied biomass from cork [27]. This behavior can be explained by the fact that some of the organic compounds present in the liquified biomass adsorb during electrolysis into the electrode's surface; hence, the solution resulting from the electrolysis process will have a lower organic load, thus increasing the emulsion's conductivity.

The second event, i.e., the shift in the oxidation peaks towards more positive potentials, was also expected, as the organic components of the emulsion are more oxidized after electrolysis. Thus, a higher potential is necessary to oxidize the remaining species. Furthermore, Figure 7 shows a third oxidation peak in the backscan of the CV of the emulsion after electrolysis. This peak could be due to the increased ionic conductivity of the solution, which indicates an increase in the diffusion coefficient, thereby increasing the transportation rate of new species susceptible to oxidation to the electrode surface.

3.2.2. Hydrogen Evolution Reaction Study

The HER was studied through LSV (Figure 8) using Pt and Ni electrodes, and then the Tafel equation (Equation (5)) was applied to the experimental data,

$$\eta = b \times \log(j) + a = (2.3RT)/(\alpha F) \times \log(-j) + (2.3RT)/(\alpha F) \times \log(-j_0) \quad (5)$$

where η is the overpotential, j is the current density, and j_0 is the exchange current density, which is defined as the current density that flows equally in equilibrium and in both ways, resulting in a zero net current and a zero net reaction rate [28]. The LSV plots recorded with Pt and Ni electrodes at 25 and 70 °C are presented in Figure 8, with the corresponding Tafel plots shown in Figure 9. The kinetic parameters obtained when applying Tafel analysis to these data are listed in Table 3.

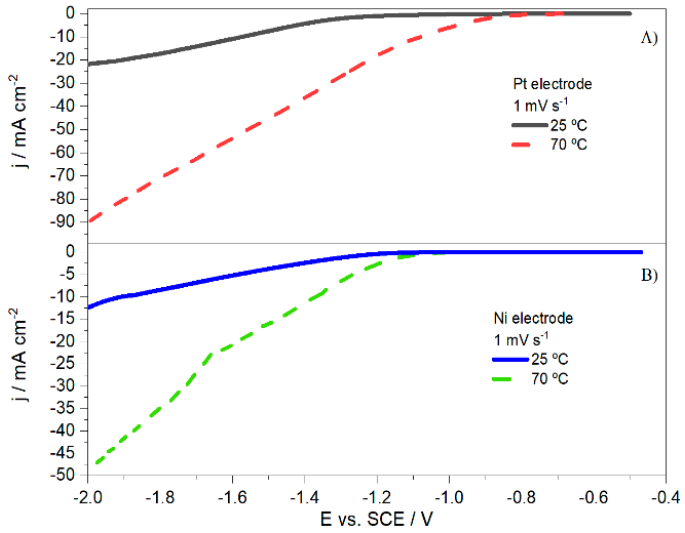

Figure 8. Linear scan voltammogram of 50/50 emulsion of liquefied biomass + 2 M KOH for studying the cathodic region using (**A**) a Pt working electrode and (**B**) a Ni working electrode at 25 and 70 °C.

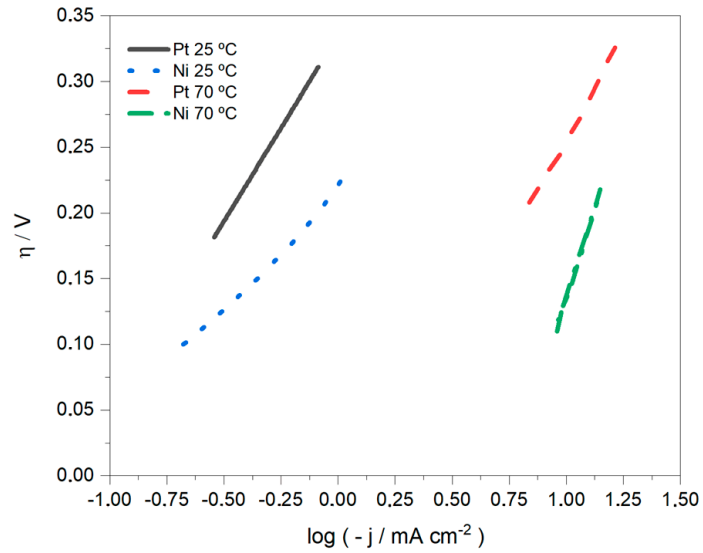

Figure 9. Tafel analysis of the HER in the 50/50 emulsion of liquefied biomass + 2 M KOH using Pt and Ni working electrodes at 25 and 70 °C.

Table 3. Kinetic parameters obtained from Tafel analysis using Pt and Ni working electrodes.

		25 °C	**70 °C**
Pt	b (mV dec^{-1})	284	319
	α	0.21	0.21
	j_0 (mA cm^{-2})	6.59×10^{-2}	1.58
Ni	b (mV dec^{-1})	180	515
	α	0.33	0.11
	j_0 (mA cm^{-2})	6.30×10^{-2}	3.14

Table 3 shows that an increase in temperature leads to an increase in both the Tafel slope (b) and the j_0 value. Although it would be desirable to see an increase in j_0 together with a decrease in the Tafel slope, the observed behavior is not uncommon. Moreover, Ghatak et al. reported the Tafel slopes obtained with Pt electrodes at 25 °C during HER in alkaline electrolyte and in eucalyptus black liquor at 113 and 135 mV dec^{-1}, and j_0 values of 1.08 and 9.86 mA cm^{-2}, respectively [29]. Comparing these j_0 values to the ones obtained in the present work, it can be concluded that the HER in these conditions (25 °C and Pt electrode) in a 50/50 emulsion of liquefied biomass + 2 M KOH is kinetically less favorable than in alkaline water or in eucalyptus black liquor, as the herein obtained j_0 value is significantly lower (6.59×10^{-2} mA cm^{-2}). However, the j_0 value significantly increases (1.58 mA cm^{-2}) when increasing the temperature to 70 °C, reaching a value slightly above that of conventional alkaline water electrolysis [29]. This has also been verified for the j_0 values obtained when using the Ni electrode. According to Shinagawa et al., the Tafel slopes using Ni electrodes typically vary between 200 and 1000 mV dec^{-1} due to the formation of Ni hydrides that limit the HER [30]. The Tafel slopes obtained herein with the Ni electrode at both temperatures fall within this range. Furthermore, the Tafel slopes for all cases are higher than 120 mV dec^{-1}, meaning that Volmer's step limits HER in this system [29,31].

3.3. Electrolysis Studies

This section of the work explores the electrolysis of the bio-oil alkaline emulsion using two different current modes, namely DC and AC (half-sinusoidal and pulsed waves) electrolysis.

3.3.1. Direct Current Electrolysis

Preliminary electrolysis tests using chronoamperometry were carried out to evaluate the most influencing variables during bio-oil alkaline emulsion electrolysis (Figure 10). These parameters were the applied cell voltage (Figure 10A), the composition of the anode material (Figure 10B), and the temperature (Figure 10C).

Figure 10A shows that increasing the cell voltage by 0.9 V, from 1.5 to 2.4 V, increases the current density from ca. 0 to 0.6 mA cm^{-2} in the stationary state. Although working at low overpotentials is usually an advantage in terms of energetic costs, these results suggest that applying a cell voltage of 2.4 V significantly benefits bio-oil alkaline emulsion electrolysis, maintaining reasonable currents even after 180 min. Figure 10B shows that Ni anodes are considerably better than TiO_2-RuO_2 anodes for this electrolysis; using Ni as both the cathode and anode generated higher current densities, making it the preferred electrode material. Figure 10C shows the influence of temperature on bio-oil alkaline emulsion electrolysis using Ni electrodes. Notably, when the temperature is increased from 25 to 50 °C, the current density in the stationary state almost doubles, rising from 2 to 7 mA cm^{-2}. Therefore, running electrolysis at temperatures higher than 25 °C is clearly beneficial.

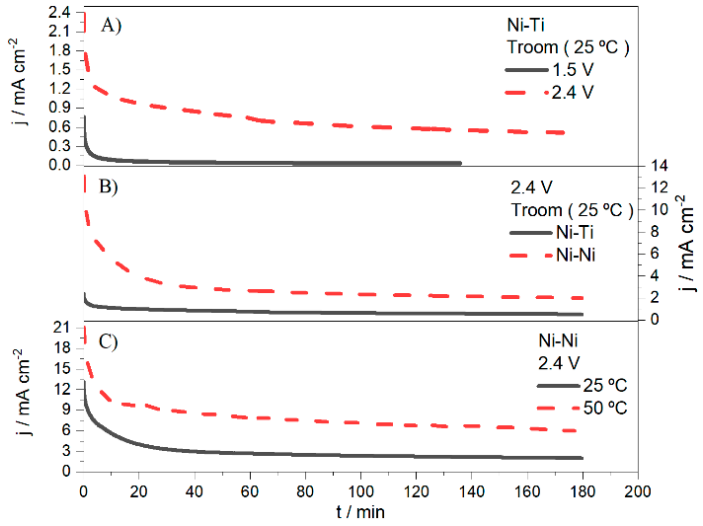

Figure 10. Electrolysis of the bio-oil alkaline emulsion under different operation conditions: (**A**) Ni cathode and TiO_2-RuO_2 anode applying 1.5 and 2.4 V at 25 °C, (**B**) Ni cathode and Ni or TiO_2-RuO_2 anodes applying 2.4 V and 25 °C, and (**C**) Ni electrodes applying 2.4 V at 25 and 50 °C.

Finally, a polarization study was conducted to evaluate the optimum electrolysis cell operating potential, considering that one goal is producing H_2. Figure 11, together with the previous LSV studies (Figure 8), confirms that for cathode polarization to reach −1.5 V and to obtain reasonable currents for the HER, it would be necessary to apply at least 2 V to the bio-oil electrolysis cell.

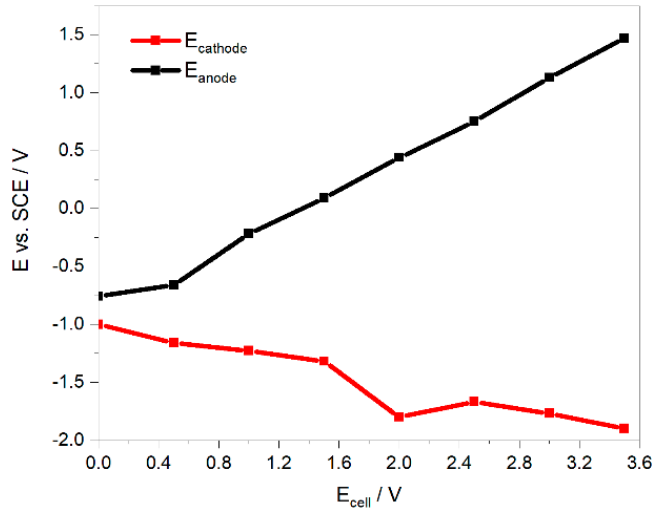

Figure 11. Polarization study with Ni electrodes in the bio-oil alkaline emulsion at 25 °C.

Subsequently, tests with Ni electrodes were conducted to optimize the electrolysis process. Results from Figure 10 and additional experiments revealed that at 2.4 V and 25 °C, no gas production occurred. Therefore, the cell potential was increased to 3 V, and the temperature was raised to 70 °C, as shown in Figure 12.

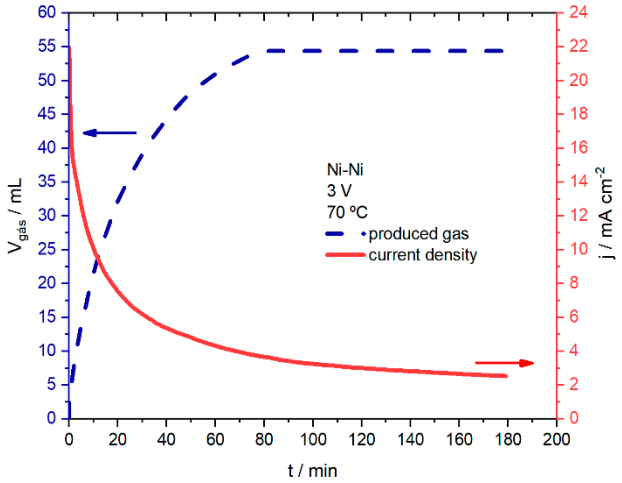

Figure 12. Gas volume and current density generated in electrolysis with Ni electrodes at 3 V and 70 °C in 3 h.

Figure 12 shows that gas production follows the same behavior as the current density, i.e., gas is produced (55 mL) during the first 80 min until the current density reaches stabilization; when the current density values stabilize, the gas production stops. To perform a quantitative analysis of these results, the Faradaic and energetic efficiencies were calculated considering that all the gas produced is H_2 (Table 4). The Faradaic efficiency was determined as the ratio of the experimentally measured H_2 volume to the theoretical H_2 volume; the latter was calculated by using the H_2 mass determined from Faraday's laws (Equations (6) and (7)) and converting it to the H_2 volume,

$$\text{1st Faraday}'\text{s law } Q = i \times t \tag{6}$$

$$\text{2nd Faraday}'\text{s law } m_{H_2} = (Q \times M)/(F \times n) \tag{7}$$

where Q is the charge in A s, i is the current in A, t is the time in s, m_{H_2} is the produced H_2 mass in g, M is the molar mass of H_2 (2.02 g mol^{-1}), and n is the number of exchanged electrons (in this case, n = 2). The energetic efficiency was determined using Equation (8),

$$\eta_{energy} = \left(\dot{n}_{H_2} \times HHV_{H_2}\right)/\dot{W}_e \tag{8}$$

where $\dot{n}_{H_2}$ is the produced H_2 flow (mol s^{-1}), HHV_{H2} is the H_2 higher heating value (286.6 kJ mol^{-1}), and $\dot{W}_e$ is the energy given to the system (kW). Direct current electrolysis (Figure 12) exhibited the highest efficiency; the calculated Faradaic and energetic efficiencies were 43 and 39%, respectively. Despite the process's innovative character, the obtained energetic efficiency is far from DOE's target of 74% for alkaline electrolyzer stacks [32].

Table 4. Electrolysis performance with Ni electrodes at 3 V for 3 h, with direct current at 70 °C, and applying pulses (300 Hz) at room temperature: theoretical H_2 production, experimentally produced gas, Faradaic efficiency, and energetic efficiency.

Test	Theoretical H_2/mL	Produced Gas/mL	$\eta_{Faradaic}$/%	$\eta_{energetic}$/%
DC	127	55	43	39
Pulsed	343	102	30	11

Electrolysis at 3 V and 60 °C using Ni electrodes and an anion-exchange membrane (AMI-7001S) was also conducted. This test revealed that gas production occurred only on the cathode side, indicating that the gas is H_2. This finding is supported by a study

conducted by Caravaca et al. [33], suggesting that organic matter oxidation, specifically lignin oxidation, occurs at a lower potential than water oxidation. Therefore, O_2 production does not occur [33]. This electrolysis test primarily confirmed the production of gas, as it showed no further improvement in current density and posed a risk of membrane fouling.

One of this study's goals was to investigate the incorporation of CO_2 into electrolysis; therefore, additional electrolysis tests were run at 3 V using Ni electrodes and bubbling CO_2. Figure 13 presents the data obtained at room temperature and 50 °C, demonstrating that under these conditions, not only are the currents low with the CO_2 bubbling, but the effect of temperature on current density is negligible, as the currents stabilize at similar values.

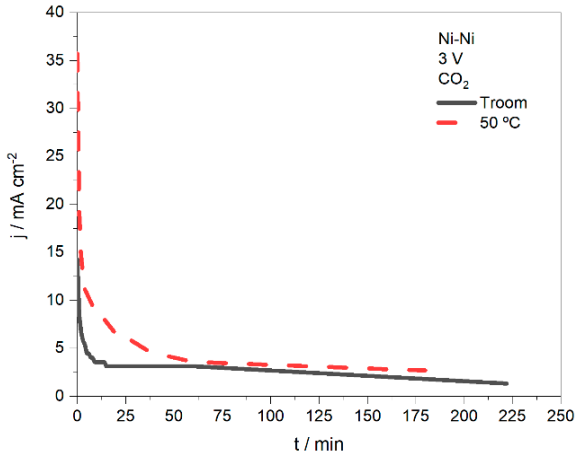

Figure 13. Current density during electrolysis with Ni electrodes, bubbling CO_2, and applying 3 V at T_{room} (17 °C) and 50 °C.

3.3.2. Alternating Current Electrolysis

Liu et al. claim that using a fluctuating current power supply can disturb the diffusion layer [34]; for this reason, some tests using this current mode were carried out. A half-sinusoidal wave was first used in these electrolysis tests to avoid electrode polarity inversion and ensure that ions moved only in one direction. So, the potential varied between 0 and a maximum of 3 V (in this case). It should be noted that in this study, the applied potential corresponds to the root mean square (RMS) value. The results showed that while the current density was higher, it was not significantly different from that generated by the continuous current tests, suggesting that electrolysis may still be limited by diffusion.

Due to the lack of a significant improvement with the half-sinusoidal AC wave, a switch to pulsed electrolysis was made. Pulsed electrolysis is known to effectively prevent the formation of the diffusion layer by interrupting the current before the layer fully develops, thereby reducing cell overpotentials [34]. Additionally, Cheng et al. reported that pulsed electrolysis can significantly enhance H_2 production efficiency at low loads, specifically by optimizing the pulse current magnitude and duty cycle [35].

Here, the pulse characteristics used were 3 V, 300 Hz, and a peak-to-peak value of 4 V. To better compare pulsed electrolysis with other current modes, Figure 14 presents a series of electrolysis tests conducted under various operating conditions to determine the optimal parameters.

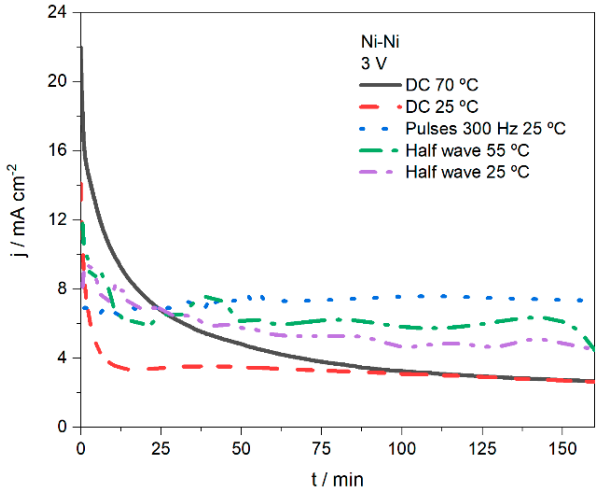

Figure 14. Current density during DC electrolysis with Ni electrodes, applying 3 V at 25 and 70 °C, using an AC half-sinusoidal wave at 25 and 55 °C, and pulses with 300 Hz at 25 °C.

Figure 14 shows that pulsed electrolysis not only produces more stable current densities but also generates significantly higher currents compared to all other electrolysis tests despite being conducted at 25 °C. Still, the amount of gas produced was the minimum amount detectable by the gas-measuring device (3.2 mL).

Another test involved bubbling CO_2 during pulsed electrolysis. Figure 15 compares the system's performance with and without CO_2 bubbling. The results show that electrolysis without CO_2 bubbling yields more stable current densities. Although higher currents were observed during the first 75 min of CO_2 bubbling, they subsequently decreased. For this reason, tests with CO_2 bubbling were abandoned at this point. The poor performance of the CO_2 bubbling and its minimal impact on electrolysis current densities, observed in both continuous current and pulsed electrolysis experiments, are mostly related to the low electrocatalytic activity of the used electrode material (i.e., nickel) for the CO_2 reduction reaction and suboptimal cathode design. The results suggest that future studies on co-electrolysis should incorporate a well-designed gas diffusion electrode that provides the required pathways for CO_2 to effectively reach the catalyst layer, ensuring a uniform flow of gas and efficient reaction kinetics at the catalyst surface.

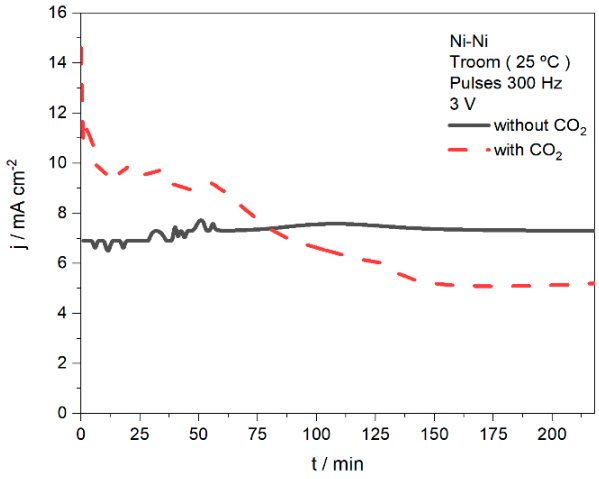

Figure 15. Current density from pulsed electrolysis with Ni electrodes at room temperature, 3 V, and 300 Hz, with and without CO_2 bubbling.

To address the low gas production observed in the pulsed electrolysis experiment shown in Figure 14, the peak-to-peak voltage was increased to 7 V while keeping the same

RMS value. Furthermore, to prevent the pulse shape from deforming over time, the circuit was modified to trigger a discharge of the diffusion layer when the potential reached 0 V. The results from these adjustments are presented in Figure 16 and Table 4.

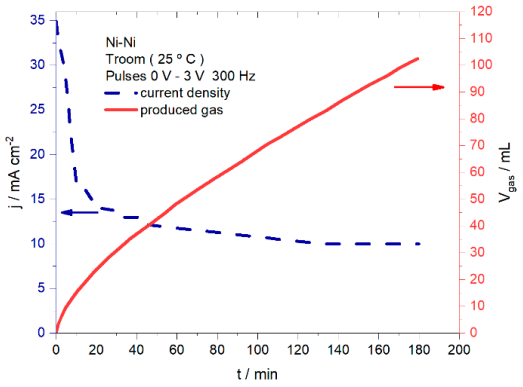

Figure 16. Current density and gas produced from pulsed electrolysis with Ni electrodes imposing a moment of 0 V at 300 Hz and room temperature.

The conditions for pulsed electrolysis shown in Figure 16 generated higher current densities, stabilizing at 10 mA cm^{-2} and producing a significantly higher amount of gas (102 mL). However, compared to direct current electrolysis tests, the calculated Faradaic and energetic efficiency were lower, at 30% and 11%, respectively. Although the electrolysis results data in Table 4 are promising, optimized operating conditions are still needed to increase the Faradaic and energetic efficiency.

3.4. Electrolysis Using Waters from the Liquefaction Process

To reuse water from the liquefaction process, bio-oil emulsions were prepared using this water source, and their performance on electrolysis was evaluated. These emulsions contained 50 vol.% of liquefied biomass in water, i.e., the condensed water and dark phase from the liquefaction process. The light-colored water phase exhibited no electrochemical activity due to its extremely low conductivity (0.01×10^{-3}, Table 1) and was therefore excluded from further tests.

Since the conductivity of the emulsions prepared with the bio-oil and each of the condensed water and dark phases from the liquefaction process was very low, 1 mL of 50 wt.% H_2SO_4 was added to increase this parameter. Figure 17 compares the results of the 3 h DC electrolysis tests using the two water phases from the liquefaction process to those of the previous alkaline emulsion (liquefied biomass + 2 M KOH).

It is clear from Figure 17 that the electrolysis run with waters from the liquefaction process led to significantly higher current densities than the alkaline emulsion. In fact, for the first hour, the current densities using the emulsion with the condensed water led to more than double the current density of the alkaline emulsion. However, after stabilization, the current values were similar to those obtained with the dark phase emulsion. Despite the promising electrolysis results obtained with the waters from the liquefaction process, these tests led to a higher Ni anode mass loss than the alkaline emulsion at the end of the 3 h test. This effect is attributed to a more corrosive acidic environment, decreasing the Ni electrode stability. Additionally, gas production should be measured to calculate the Faradaic and energetic efficiencies and evaluate whether this approach, using the waters from the liquefaction process, is economically worth it.

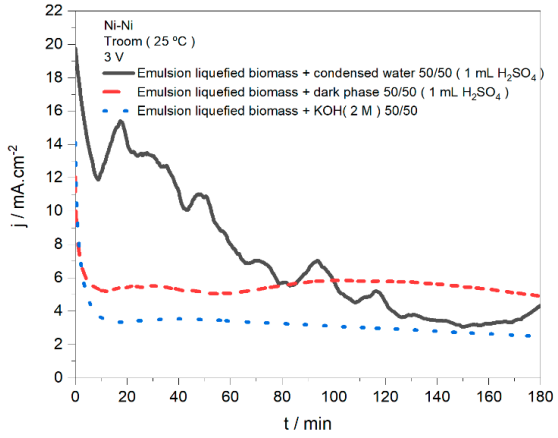

Figure 17. Current density from electrolysis with Ni electrodes when applying 3 V at room temperature with different 50/50 emulsions: liquefied biomass + condensed water/dark phase/2 M KOH.

4. Conclusions

The main goals of this study were to optimize the electrolysis of liquefied biomass to produce H_2, produce value-added compounds through the oxidation of organic matter, and capture CO_2 in the electrolysis medium. Since little information exists about the electrochemical activity of liquefied biomass (and consequently about the prepared emulsions), preliminary electrochemical studies, including CV and LSV, were conducted.

From CV, it was verified that the organic matter in the liquefied biomass is susceptible to redox reactions. Comparing CVs from the bio-oil emulsion before and after electrolysis, one can notice an increase in the current density, a deviation of peaks towards more positive potentials, and the appearance of a third anodic peak. The first observation indicates that this is due to the loss of some organic compounds that adsorb into the electrodes; the second indicates that the emulsion after electrolysis is more oxidized; and the third is due to an increase in the emulsion's conductivity. The HER study in the bio-oil emulsion, using a Pt electrode, demonstrated that the reaction is more kinetically hindered than in alkaline water or black liquor.

Preliminary electrolysis tests with direct current showed that a potential higher than 2 V is required to attain reasonable current densities. Additionally, Ni electrodes perform better than TiO_2-RuO_2 alloy electrodes, and a temperature higher than room temperature is beneficial for electrolysis. The best result from the direct current electrolysis tests involved applying 3 V and 70 °C with Ni electrodes, leading to a 39% energetic efficiency and a 43% Faradaic efficiency. Although the electrolysis results are promising, the energetic efficiency of the process is still far from the ultimate (i.e., by 2031) DOE target for liquid alkaline electrolyzer stacks, which has been set as 74%.

The electrolysis test that produced a higher gas volume was carried out with a pulsed current of 300 Hz at 3 V and room temperature; this test had 11% energetic efficiency and 30% Faradaic efficiency. Additional electrolysis tests involving the bubbling of CO_2 into the bio-oil emulsion showed no significant improvement in the recorded current densities, both in the direct current and pulsed electrolysis modes. On the other hand, incorporating water from the liquefaction process showed higher current densities during electrolysis; however, an increased Ni electrode mass loss was verified.

This study demonstrates a promising approach to producing H_2 without O_2 contamination, addressing a critical challenge in H_2 production. However, the further optimization of operating conditions is required to enhance efficiency and scalability. Additionally, more in-depth investigations are necessary to identify the added-value compounds generated

during organic matter oxidation and to further evaluate whether CO_2 bubbling could facilitate the formation of other valuable gases (e.g., CO, CH_4).

Author Contributions: Conceptualization, M.M.M. and D.M.F.S.; methodology, A.P.R.A.F.; validation, M.M.M. and D.M.F.S.; formal analysis, A.P.R.A.F.; investigation, A.P.R.A.F.; resources, D.M.F.S.; data curation, A.P.R.A.F., M.M.M. and D.M.F.S.; writing—original draft preparation, A.P.R.A.F.; writing—review and editing, D.M.F.S.; supervision, M.M.M. and D.M.F.S. All authors have read and agreed to the published version of the manuscript.

Funding: Fundação para a Ciência e a Tecnologia (FCT, Portugal) is acknowledged for funding a Principal Researcher contract (2023.09426.CEECIND) in the scope of the Individual Call to Scientific Employment Stimulus–6th Edition (D.M.F.S).

Data Availability Statement: The original contributions presented in this study are included in the article. Further inquiries can be directed to the corresponding author.

Conflicts of Interest: The authors declare no conflicts of interest.

References

1. Mckendry, P. Energy production from biomass (part 1): Overview of biomass. *Bioresour. Technol.* **2002**, *83*, 37–46. [CrossRef]
2. Brandt, A.; Gräsvik, J.; Hallett, J.P.; Welton, T. Deconstruction of lignocellulosic biomass with ionic liquids. *Green Chem.* **2013**, *15*, 550–583. [CrossRef]
3. Nabgan, W.; Tuan Abdullah, T.A.; Mat, R.; Nabgan, B.; Gambo, Y.; Ibrahim, M.; Ahmad, A.; Jalil, A.; Triwahyono, S.; Saeh, I. Renewable hydrogen production from bio-oil derivative via catalytic steam reforming: An overview. *Renew. Sustain. Energy Rev.* **2017**, *79*, 347–357. [CrossRef]
4. Carvalho, R. Cork Liquefaction: Improvement of the Process and Its Application on Adhesives Formulation. Master's Thesis, Universidade de Lisboa, Lisbon, Portugal, 2015.
5. Akhtar, J.; Amin, N.A.S. A review on process conditions for optimum bio-oil yield in hydrothermal liquefaction of biomass. *Renew. Sustain. Energy Rev.* **2011**, *15*, 1615–1624. [CrossRef]
6. Kim, J.Y.; Lee, H.W.; Lee, S.M.; Jae, J.; Park, Y. Overview of the recent advances in lignocellulose liquefaction for producing biofuels, bio-based materials and chemicals. *Bioresour. Technol.* **2019**, *279*, 373–384. [CrossRef] [PubMed]
7. Zhang, X.; Chan, S.H.; Ho, H.K.; Tan, S.; Li, M.; Li, G.; Li, J.; Feng, Z. Towards a smart energy network: The roles of fuel/electrolysis cells and technological perspectives. *Int. J. Hydrogen Energy* **2015**, *40*, 6866–6919. [CrossRef]
8. Chi, J.; Yu, H. Water electrolysis based on renewable energy for hydrogen production. *Cuihua Xuebao/Chin. J. Catal.* **2018**, *39*, 390–394. [CrossRef]
9. Arcos, J.M.M.; Santos, D.M.F. The hydrogen color spectrum: Techno-economic analysis of the available technologies for hydrogen production. *Gases* **2023**, *3*, 25–46. [CrossRef]
10. Zhang, Y.; Guo, S.X.; Zhang, X.; Bond, A.; Zhang, J. Mechanistic understanding of the electrocatalytic CO_2 reduction reaction—New developments based on advanced instrumental techniques. *Nano Today* **2020**, *31*, 100835. [CrossRef]
11. Liang, S.; Altaf, N.; Huang, L.; Gao, Y.; Wang, Q. Electrolytic cell design for electrochemical CO_2 reduction. *J. CO_2 Util.* **2020**, *35*, 90–105. [CrossRef]
12. Ferreira, A.P.R.A.; Oliveira, R.C.P.; Mateus, M.M.; Santos, D.M.F. A review of the use of electrolytic cells for energy and environmental applications. *Energies* **2023**, *16*, 1593. [CrossRef]
13. Khan, M.A.; Al-Attas, T.; Roy, S.; Rahman, M.M.; Ghaffour, N.; Thangadurai, V.; Larter, S.; Hu, J.; Ajayan, P.M.; Kibria, M.G. Seawater electrolysis for hydrogen production: A solution looking for a problem? *Energy Environ. Sci.* **2021**, *14*, 4831–4839. [CrossRef]
14. Yu, Z.; Li, Y.; Martin-Diaconescu, V.; Simonelli, L.; Ruiz Esquius, J.; Amorim, I.; Araujo, A.; Meng, L.; Faria, J.L.; Liu, L. Highly efficient and stable saline water electrolysis enabled by self-supported nickel-iron phosphosulfide nanotubes with heterointerfaces and under-coordinated metal active sites. *Adv. Funct. Mater.* **2022**, *32*, 2206138. [CrossRef]
15. Yu, Z.; Liu, L. Recent advances in hybrid seawater electrolysis for hydrogen production. *Adv. Mater.* **2024**, *36*, 2308647. [CrossRef]
16. Dolle, C.; Neha, N.; Coutanceau, C. Electrochemical hydrogen production from biomass. *Curr. Opin. Electrochem.* **2022**, *31*, 100841. [CrossRef]
17. Umer, M.; Brandoni, C.; Jaffar, M.; Hewitt, N.J.; Dunlop, P.; Zhang, K.; Huang, Y. An experimental investigation of hydrogen production through biomass electrolysis. *Processes* **2024**, *12*, 112. [CrossRef]
18. Guerra, L.; Moura, K.; Rodrigues, J.; Gomes, J.; Puna, J.; Bordado, J.; Santos, T. Synthesis gas production from water electrolysis, using the Electrocracking concept. *J. Environ. Chem. Eng.* **2018**, *6*, 604–609. [CrossRef]

19. Nunes, A.M.; Bordado, J.C.M.; Neiva Correia, J.; Mateus, M.M.; Oliveira, F.M.; Galhano, R.M. Catalytic and Continuous Thermochemical Process of Production of Valuable Derivatives from Organic Materials and/or Waste. WO2021245440, 2 June 2020. Available online: https://patentscope2.wipo.int/search/pt/detail.jsf?docId=WO2021245440&_cid=JP1-M4N672-18620-1 (accessed on 13 January 2025).
20. Silva, T.; Condeço, J.; Santos, D.M.F. Preliminary studies on the electrochemical conversion of liquefied forest biomass. *Reactions* **2022**, *3*, 553–575. [CrossRef]
21. Pacheco, W.F.; Semaan, F.S.; Almeida, V.G.K.; Ritta, A.; Aucélio, R. Voltammetry: A brief review about concepts. *Rev. Virtual Quim.* **2013**, *5*, 516–537. [CrossRef]
22. Elgrishi, N.; Rountree, K.J.; McCarthy, B.D.; Rountree, E.; Dempsey, J. A Practical Beginner's Guide to Cyclic Voltammetry. *J. Chem. Educ.* **2018**, *95*, 197–206. [CrossRef]
23. Espinoza, E.M.; Clark, J.A.; Soliman, J.; Derr, J.M.; Vullev, V. Practical Aspects of Cyclic Voltammetry: How to Estimate Reduction Potentials When Irreversibility Prevails. *J. Electrochem. Soc.* **2019**, *166*, H3175–H3187. [CrossRef]
24. Li, D.; Lin, C.; Batchelor-McAuley, C.; Lifu, C.; Richard, C. Tafel analysis in practice. *J. Electroanal. Chem.* **2008**, *826*, 117–124. [CrossRef]
25. Santos, D.M.F.; Sequeira, C.A.C. Cyclic voltammetry investigation of borohydride oxidation at a gold electrode. *Electrochim. Acta* **2010**, *55*, 6775–6781. [CrossRef]
26. Cardoso, D.S.P.; Santos, D.M.F.; Šljukić, B.; Sequeira, C.; Macciò, D.; Saccone, A. Platinum-rare earth cathodes for direct borohydride-peroxide fuel cells. *J. Power Sources* **2016**, *307*, 251–258. [CrossRef]
27. Silva, T. Electrochemical Conversion of Liquefied Forest Biomass. Master's Thesis, Instituto Superior Técnico, Lisbon, Portugal, 2018.
28. Bard, A.J.; Faulkner, L.R. *Electrochemical Methods*, 2nd ed.; John Wiley & Sons, Inc.: Hoboken, NJ, USA, 2001.
29. Ghatak, H.R.; Kumar, S.; Kundu, P.P. Electrode processes in black liquor electrolysis and their significance for hydrogen production. *Int. J. Hydrogen Energy* **2008**, *33*, 2904–2911. [CrossRef]
30. Shinagawa, T.; Garcia-Esparza, A.T.; Takanabe, K. Insight on Tafel slopes from a microkinetic analysis of aqueous electrocatalysis for energy conversion. *Sci. Rep.* **2015**, *5*, 13801. [CrossRef] [PubMed]
31. Caravaca, A.; Garcia-Lorefice, W.E.; Gil, S.; Lucas-Consuegra, A.; Vernoux, P. Towards a sustainable technology for H_2 production: Direct lignin electrolysis in a continuous-flow polymer electrolyte membrane reactor. *Electrochem. Commun.* **2019**, *100*, 43–47. [CrossRef]
32. U.S. Department of Energy. *Technical Targets for Liquid Alkaline Electrolysis*. Available online: https://www.energy.gov/eere/fuelcells/technical-targets-liquid-alkaline-electrolysis (accessed on 14 January 2025).
33. Vincent, I.; Choi, B.; Nakoji, M.; Ishizuka, M.; Tsutsumi, K.; Tsutsumi, A. Pulsed current water splitting electrochemical cycle for hydrogen production. *Int. J. Hydrogen Energy* **2018**, *43*, 10240–10248. [CrossRef]
34. Liu, T.; Wang, J.; Yang, X.; Gong, M. A review of pulse electrolysis for efficient energy conversion and chemical production. *J. Energy Chem.* **2021**, *59*, 69–82. [CrossRef]
35. Cheng, H.; Xia, Y.; Hu, Z.; Wei, W. Optimum pulse electrolysis for efficiency enhancement of hydrogen production by alkaline water electrolyzers. *Appl. Energy* **2024**, *358*, 122510. [CrossRef]

Disclaimer/Publisher's Note: The statements, opinions and data contained in all publications are solely those of the individual author(s) and contributor(s) and not of MDPI and/or the editor(s). MDPI and/or the editor(s) disclaim responsibility for any injury to people or property resulting from any ideas, methods, instructions or products referred to in the content.